

2013

Plasma MHD Activity Observations via Magnetic Diagnostics.

GOMTRAIC 2013



Plasma MHD Activity Observations via Magnetic Diagnostics

F.Ostyn* M.R. Ramos** D.H.Arriaga***

10 de mayo de 2013

Índice

1. Introduction	2
2. Basics of the theory	2
2.1. Plasma & Fusion	2
2.2. Magnetic confinement: Tokamak	4
2.3. GOLEM	5
2.4. Magnetics Islands	7
3. Principles of the measurement	9
4. Measurement setup	11
5. Data processing methods	13
5.1. Fluctuation of raw data analysis (theta-time diagram)	13
5.2. Spectrogram	16
5.3. Cross correlation analysis	18
6. Results	20
7. Discussion	21
8. Appendix	22
8.1. Appendix I	22
8.1.1. Safety Factor	22
8.2. Appendix II	24
8.2.1. Frederyk's Scripts	24
8.3. Appendix III	28
8.3.1. List of	28
9. Bibliography	29

*UGent

**University of Seville

***CICATA-IPN

... somewhere, in the ancient cellars of Prague, there is hidden indeed **infernal power**. Yet it is the very of **power celestial stars** themselves. Calmly dormant, awaiting mankind to discover **the magic key**, to use this power for their benefit...

1. Introduction

In a lot of plasma experiments, the main parameters of the experiment consist of the magnitude of currents and magnetic and electric fields inside and outside the plasma volume.

Reliable measurement of these parameters is basic to performing and understanding the experiments. Moreover, in many cases, measurements of these global quantities can give considerable information about the microscopic properties of the plasma such as temperature, density, and composition. It is therefore logical to begin our consideration of the topic of plasma diagnostic by consideration of magnetic techniques.

The GOMTRAIC 2013 MHD team measured the mode number of magnetic islands appearing in the plasma of GOLEM tokamak using magnetic diagnostics. In this report, basic theory, measurement setup and results are presented.

2. Basics of the theory

2.1. Plasma & Fusion

It is projected that the global energy demands will have a rise of 40 % between 2009 and 2035 [1] [2]. Furthermore it is very likely that greenhouse gases (e.g. CO_2), which are a substantial by product in the combustion of fossil fuels, have a climate-changing effect . By the end of the century there may be the need for a technology producing a significant amount of energy in an environmentally friendly and economical way.

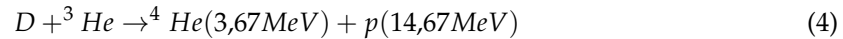
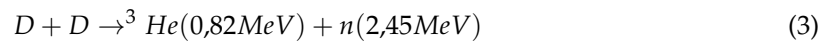
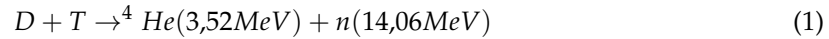
The alternative energy sources: sun, wind, tide and hydro-energy are subject to the local weather conditions. Therefore they cannot be considered as the full substitution for commonly used fossil fuels.

In the 20th century it was discovered a new form of energy, nuclear energy. Nuclear energy is gained in two processes: fission and fusion. The fission energy is gained from the splitting up heavy elements, e.g. uranium or thorium and nowadays there are about 400 fission reactors all over the world.

The fusion of light elements, especially hydrogen isotopes is the way in which the stars obtains their energy ,has the potential of providing an essentially unlimited source of energy.

Human beings have been searching a long time for a way to reproduce such a source of energy on Earth. The cross-section for the whole cycle in the stars due to the weak interaction involved in reaction is too low to be reproduced on Earth (the Stars overcomes this problem by its huge mass).

The fusion reactions of most practical interest for terrestrial fusion power production [3] [4] [12] are:



To initialize and preserve reactions in thermonuclear reactor the particles need to be heated to high energies, in the range of tens of keV to overcome the repulsive Coulomb force. Under this temperature, matter goes into state of plasma.

There are two categories of plasma (and also plasma physics): hot and cold plasmas. In the cold plasmas only a small fraction of the atoms is ionized, the temperature of gas is low (2 eV). In the hot plasmas full ionization takes place, and the particles are in thermal equilibrium with the temperature 10 - 10 000 eV. When the temperature is high enough ($T \geq 5\text{keV}$), the particles are able to pass Coulomb barrier, so the hot plasma is suitable background for the fusion.

For using fusion as a source of energy (positive energy gain), a relation among plasma parameters, termed the Lawson criterion [5], must be fulfilled:

$$L = n\tau_E T_i > C_{crit} \quad (5)$$

where n is the plasma density, T_i is the ion temperature and the definition of τ_E depends on the approach to the fusion; roughly it is the time when the thermonuclear reactions can take place. For different reactions C_{crit} is different, for example for the D-T reaction, the $C_{crit} \approx 5 * 10^{21} \text{keV m}^{-3}$. In order to build up a fusion reactor, we are looking for a compromise among density, energy confinement time, and temperature.

Nowadays, two methods of confinement are investigated in fusion research to reach an ignited plasma.:

- Lasers (inertial fusion): High density and short confinement time. A solid D-T sphere (pellet) is heated by a laser or a heavy ion beam. Very high n is achieved by this approach, however only for a very short time τ_E .
- Magnetic devices (closed systems - toruses): Low density and long confinement time, use magnetic confinement to improve parameters in Lawson criterion, especially τ_E at modest level of n and T_i .

2.2. Magnetic confinement: Tokamak

On principle, tokamak [4] [12] [13] is a ring-shaped vacuum vessel placed as the secondary circuit of a transformer. Plasma is confined inside by a strong magnetic field (toroidal and poloidal magnetic fields) along the chamber.

The vessel, torus, has two symmetry axes: major and minor to characterize two basic directions: toroidal which is parallel to the minor axis and poloidal which is azimuthal to the minor axis. Another important geometrical parameters are minor radius (shortest distance between the minor axis and the edge of a torus) and major radius (shortest distance between major and minor axis).

Since the plasma is an electrical conductor, it is possible to heat the plasma by inducing a current through it; in fact, the induced current that heats the plasma usually provides most of the poloidal field. The current is induced by slowly increasing the current through an electromagnetic winding linked with the plasma torus: the plasma can be viewed as the secondary winding of a transformer. (figure 1).

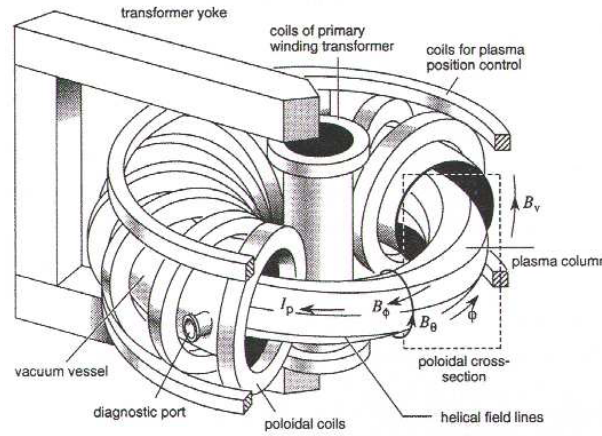


Figura 1: Tokamak configuration scheme.

This plasma current I_p produces a poloidal magnetic field B_θ . Solenoid coils (toroidal field coils) wound around the torus creates a strong toroidal magnetic field B_ϕ . The resultant magnetic field is helically shaped and its lines form nested closed magnetic surfaces. Degree of helicity is characterized by dimensionless parameter called safety factor q [6].

The $q(r)$ is the number of toroidal turns it takes a magnetic field line to encircle the full poloidal circumference of the torus. For tokamak with a circular cross-section¹ it is defined as

$$q(r) = \frac{r}{R} \frac{B_\phi}{B_\theta} \xrightarrow{\text{GOLEM}} q(r=a) \approx 90,3 \frac{B_\phi}{I_p} \quad (6)$$

For the stability of plasma column there are quadrupole coils for plasma position control, that create vertical and horizontal magnetic fields.

¹Appendix I

2.3. GOLEM

The GOLEM tokamak [8] [9] [10] [11] is a tokamak with a circular cross section and with full remote control capability and educational purpose. It's a small sized tokamak device equipped with basic controls and diagnostics (table 1 and figure 2).

Cuadro 1: *GOLEM: Dimensions and Parameters*

Major radius R	0.4 m	Minor radius r	0.1 m
Radial position of the limiter	0.085 m	Toroidal magnetic field B_Φ	<0.8 T
Toroidal plasma current I_p	<8 kA	Safety Factor at Edge $q(a)$	15
Pulse length t	<13ms	Background Pressure of Vacuum P	10-200 mPa
Central electron temperature T_e	<80 eV	Work Gas	H_2

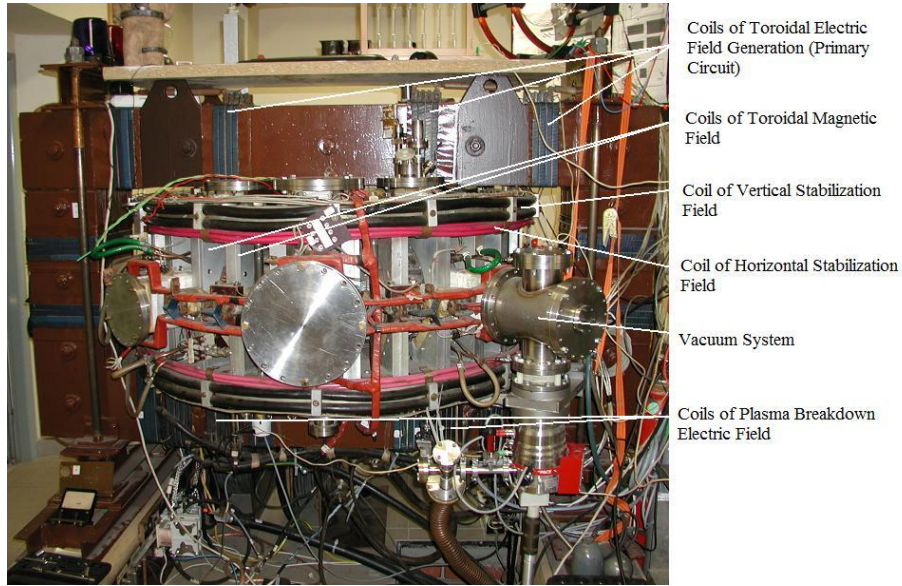


Figura 2: *Front view of the GOLEM tokamak.*

Before discharge, the vacuum vessel is evacuated down to the work pressure and filled by working gas (hydrogen).

After that, the power supplies are connected to the toroidal magnetic field coils. Since now, the toroidal magnetic field B_Φ starts increasing. When B_Φ reaches a certain valor, the primary transformer winding is automatically connected to its power supplies (capacitor banks) and the toroidal electric field E_Φ is induced within the vacuum vessel. The $E_\Phi = \frac{U_{loop}}{2\pi R}$ starts to accelerate free electrons², which are produced by an electron gun placed in the limiter shadow.

²Free electrons are always present due to the cosmic radiation, but their amount is not sufficient for a reproducible breakdown (the moment of ignition of the discharge)

After breakdown, the electron density n_e increases exponentially.

After several ms from breakdown, the working gas is completely ionized. Simultaneously, the plasma current I_p increases, which is determined by the primary circuit parameters. The slope $\frac{dI_p}{dt}$ has to be kept relatively low to negate the skin effect, which could drive the current only on the surface of the plasma column and plasma gets unstable and disrupts.

After the plasma current reaches values of $\approx 5-8$ kA, it tends to remain constant for the next ≈ 5 ms. During this quasistationary phase of discharge, the loop voltage is 2-3 V. The quasistationary phase is exploited for physical measurements. After ms, the primary winding of the transformer is set to be short circuited. The plasma current exponentially decays (figure 3).

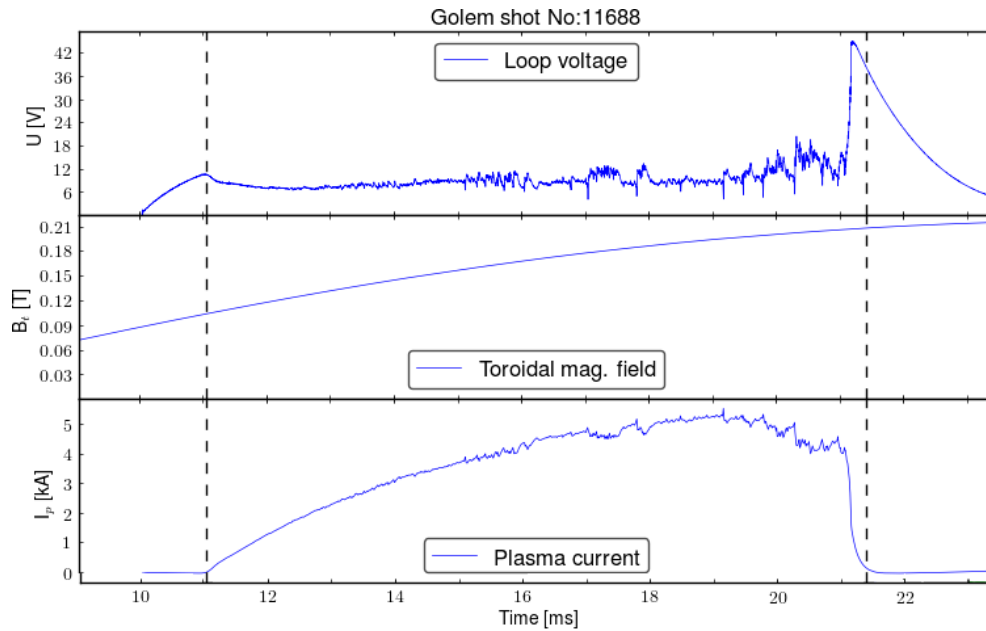


Figure 3: Temporal evolution of a typical GOLEM discharge, with parameters: loop voltage (U_{loop}) toroidal magnetic field (B_Φ) and plasma current (I_p). The whole discharge is plotted. Blue vertical lines indicate the beginning and the end of the discharge.

Fusion plasma is a source of many instabilities that deteriorate confinement of particles and energy. There are two main types of instabilities occurring in plasmas:

- Magnetic instabilities: The magnetohydrodynamics (MHD) instabilities occur at the radii where safety factor has rational value $q(r) = m/n$ and they can even create layers where the magnetic field is fully ergodized, which strongly deteriorates plasma confinement.
- Electrostatic instabilities: Electrostatic turbulence is dominant at the plasma edge and it demonstrates itself by fluctuations of plasma density and potential.

2.4. Magnetics Islands

Magnetohydrodynamics (MHD) studies the dynamics of electrically conducting fluids, like plasma. MHD provides a good theoretical framework to describe inhomogeneities such as magnetic islands [4] [7] [17]. They are present where the poloidal magnetic field flux is perturbed. At the top of the figure 4, a cross section was taken of the nested poloidal magnetic flux surfaces.

With long axial plasma column with circular cross section, plasma current is constant only if there is no B_t gradient, thus no Shafranov shift. After all, poloidal flux surfaces in general are solution of Grad-Shafranov equation, which originates from:

$$\nabla p = \mathbf{j} \times \mathbf{B} \quad (7)$$

On these surfaces, poloidal magnetic field flux, pressure (p), temperature (T) and plasma current (J) are constant. If inhomogeneities are present, the situation changes to the one present at the bottom of the figure 4. Now p, T and J are short circuited where the lines intersect. As this changes plasma behavior, it is important to know where and when this happens.

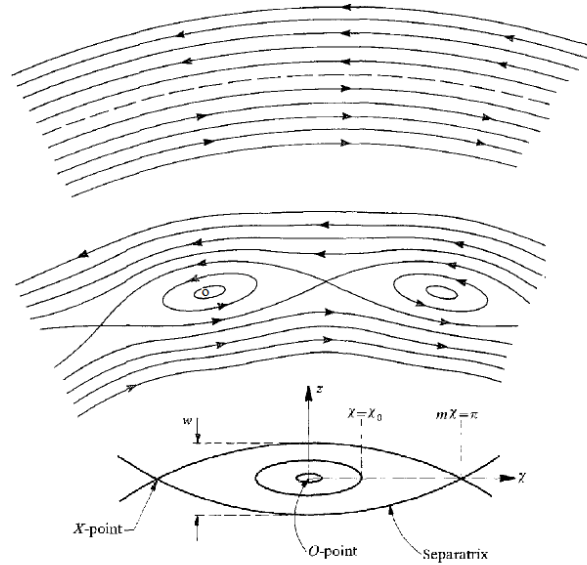


Figure 4: Contour plot of $m \geq 2$ island in the R - Z plane. The O -point, the X -point and the (full) island width w are indicated.

These islands manifest at low safety factor q , a key parameter in MHD. The safety factor is then equal to m/n , where m and n are natural numbers.

As for GOLEM tokamak, n can be put equal to one, islands will appear if $q = m$.

Mode number m then corresponds to the number of intersections defined above. For example, for $m = 3$ we get a poloidal cross section of the plasma's poloidal magnetic field lines like the one at figure 5.

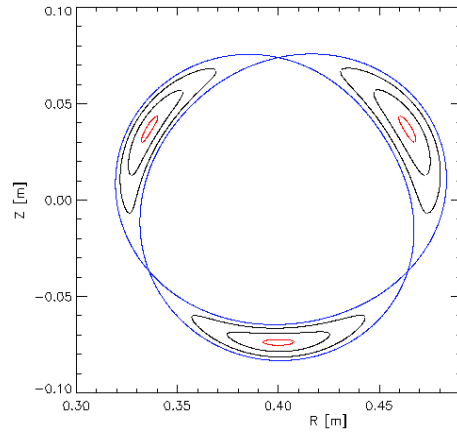


Figure 5: Island flux surfaces

The tokamak is equipped with a basic diagnostic system for measuring key plasma parameters.[8] [9] [10]

- A single loop surrounding the transformer core measures the loop voltage U_{loop} .
- A Rogowski coil surrounding the tokamak chamber measures the sum of the plasma and chamber current $I_{(p+ch)}$.
- A small pick-up coil placed on the tokamak chamber detects the toroidal magnetic field B_{tor} .
- A photodiode which faces a glass port of the tokamak detects the plasma radiation from the emitted visible spectra.

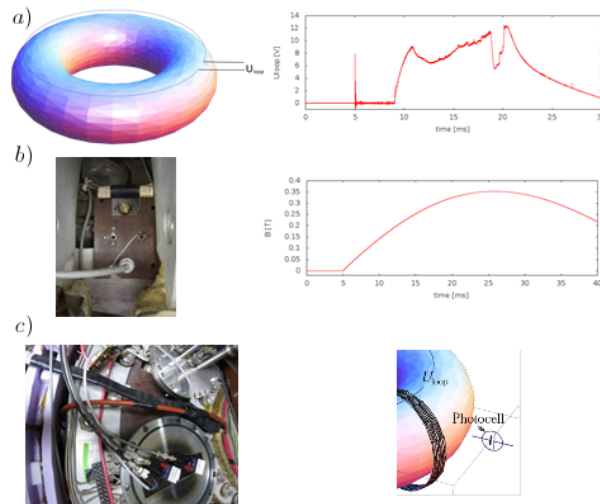


Figure 6: Basic parameter measurements: a) U_{loop} measurements and result, b) B_{tor} measurement and result, c) $I_{(p+ch)}$ and plasma radiation measurement

3. Principles of the measurement

Structure of magnetohydrodynamic (MHD) modes has always been a study of interest in tokamak devices . It is well known that Mirnov oscillations with poloidal and toroidal mode numbers m and n , respectively, are created by perturbation of current channel on rational magnetic surfaces. The coherent structure of such rotating modes can be obtained by poloidal and toroidal arrays of Mirnov coils.

In GOLEM, array of 16 magnetic probe (Mirnov coils) are installed to detect poloidal magnetic field B_θ inside the vacuum vessel [17].

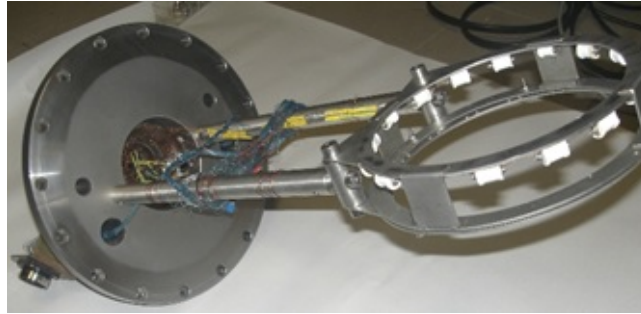


Figure 7: Set of 16 Mirnov coils mounted in a poloidal ring to work like sensors of local magnetic field.

Magnetic coil is used like a inductive sensor for magnetic field measurement based on Maxwell equations [15] [13]. In a region free of charges ($\rho = 0$) and no currents ($J = 0$), such as in a vacuum, Maxwell's equations reduce to:

$$\nabla \cdot \mathbf{E} = 0 \quad \text{Gauss's law} \quad (8)$$

$$\nabla \times \mathbf{E} = -\frac{\partial \mathbf{B}}{\partial t} \quad \text{Maxwell-Faraday law} \quad (9)$$

$$\nabla \cdot \mathbf{B} = 0 \quad \text{Gauss's law for magnetism} \quad (10)$$

$$\nabla \times \mathbf{B} = \mu_0 \mathbf{J} + \frac{1}{c^2} \frac{\partial \mathbf{E}}{\partial t} \quad \text{Ampere's circuital law} \quad (11)$$

where c is the speed of light in vacuum.

Even though magnetic coil is used as a magnetic field sensor, it measures rate of change of magnetic induction B_θ instead of the quantity itself. This is because its principle of operation is based on integral form of Faraday's law.

The Maxwell - Faraday law establish that a time-varying magnetic field is always accompanied by a spatially-varying, non-conservative electric field, and vice-versa.

$$\nabla \times \mathbf{E} = -\frac{\partial \mathbf{B}}{\partial t} \quad (12)$$

where $\nabla \times$ is the curl operator and again $\mathbf{E}(r, t)$ is the electric field and $\mathbf{B}(r, t)$ is the magnetic field.

It can also be written in an integral form by the Stokes theorem

$$\oint_{\partial\Sigma} \mathbf{E} \cdot d\mathbf{l} = - \int_{\Sigma} \frac{\partial \mathbf{B}}{\partial t} \cdot d\mathbf{A} \quad (13)$$

where Σ is a surface bounded by the closed contour $\partial\Sigma$, E is the electric field, B is the magnetic field, $d\mathbf{l}$ is an infinitesimal vector element of the contour $\partial\Sigma$, $d\mathbf{A}$ is an infinitesimal vector element of surface Σ .

The integral on the left-hand side is the electric potential or voltage \hat{V} in Volts induced at the ends of the wire of coil and is equals the rate of change of $\Phi = \int B \cdot dS$ in Webers per second (product of effective area of coil S and time-derivation of averaged magnetic field magnitude in the coil B), thus mean value of B can be obtained from equation:

$$\hat{V} = - \frac{d\Phi}{dt} \quad (14)$$

Such a magnetic coil, illustrated in the figure, may be considered the archetype of magnetic measurements. In a uniform magnetic field, varying with time $B(t)$, the voltage induced in the coil is

$$\hat{V} = -NA \frac{dB}{dt} = -A_{eff} \frac{dB}{dt} \rightarrow dB = - \frac{1}{A_{eff}} \hat{V} dt \quad (15)$$

where $\Phi = B(t)NA = B(t)A_{eff}$ is the magnetic flux, N is the number of turns in the coil of area A and A_{eff} is the effective surface of each coils.

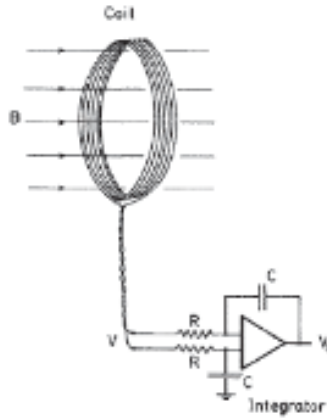


Figura 8: Typical magnetic coil and integrating circuit

As indicated in the figure, because one is interested in B rather than \dot{B} , therefore analog integrating circuit, such as the one show, is generally used to obtain a signal proportional to the field.

4. Measurement setup

There are currently 16 Mirnov coils placed on a circular rack, put inside of liner. Locations of respective coils are depicted in fig. 9.

Coils are placed on minor radius of 93.5 mm. Although Mirnov coils are used for measurement of poloidal field.

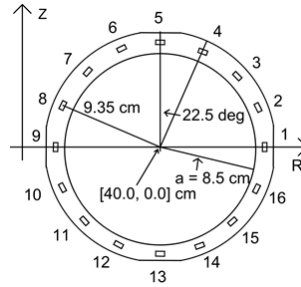


Figura 9: On tokamak GOLEM, Mirnov coils is term used for small coils of local poloidal magnetic field measurement, placed inside of liner. The main purpose of Mirnov coils is for plasma MHD activity measurements.

There are three stated requirements that have to be met, for magnetic coil to become a reliable sensor of magnetic field [16]:

- Have minimal perturbing effect on plasma column.
- Sufficient sensitivity to overcome electric noise associated with electronics devices.
- High frequency response to follow rapid magnetics fluctuations.

However, these conditions are in conflict with each other, since in order to rise sensitivity of sensor, effective area of the coil has to rise as well. For better frequency response, this area has to be in configuration of less numerous large loops, rather than large number of small loops. This, however, collides with the requirement of minimal perturbing effect on plasma. The effective area and polarity of all sensitivity of sensor [17] are shown in the table 2.

Cuadro 2: Characterization of Mirnov Coils

Coil #	Polarity	A_{eff} [cm^2]	θ [$^\circ$]	Coil #	Polarity	A_{eff} [cm^2]	θ [$^\circ$]
1	-	68.93	0	9	-	67.62	180
2	-	140.68	22.5	10	+	142.80	202.5
3	+	138.83	45	11	-	140.43	225
4	+	140.43	67.5	12	x	x	247.5
5	-	68.59	90	13	x	x	270
6	+	134.47	112.5	14	x	x	292.5
7	-	134.28	135	15	-	139.82	315
8	+	142.46	157.5	16	-	139.33	337.5

In a uniform magnetic field, varying with time $B(t)$, the voltage induced in each coil is

$$\hat{V} = -NA \frac{dB}{dt} = -A_{eff} \frac{dB}{dt} \quad (16)$$

Experimentally $\hat{V} : \hat{V}(i)$ is a discrete signal and that voltage \hat{V} obtained by the sensor will have to be integrated in order to obtain measured quantity of B.

$$B(t) \approx -\frac{\Delta t}{A_{eff}} \sum_i \hat{V}(i) \quad (17)$$

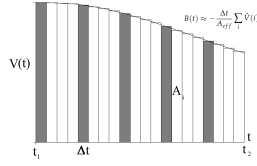


Figure 10: Numerical integration consists of finding numerical approximations for the value A_i

where Δt is the sampling time. Integrated magnetic measurements are very sensitive to the DC bias of the measurement circuit [14], which needs to be corrected. If the sampling rate is 1 MHz, and the shot starts at 5 ms, we have 5000 samples from the background noise.

$$\hat{V}(i) = V_{measured}(i) - \frac{1}{5000} \sum_{i=1}^{5000} V_{measured}(i) \quad (18)$$

The poloidal magnetic field perturbation can be obtained by the elimination of the smooth signal from the original signal of the magnetic field.

$$B_{per}(t) = B(t) - \text{smooth}(B(t)) \quad (19)$$

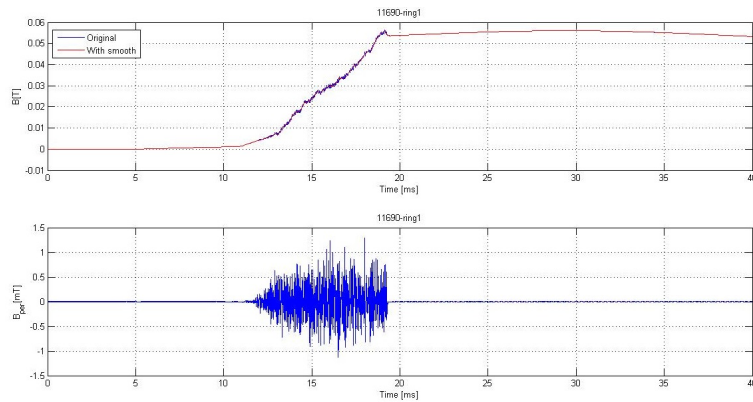


Figure 11: Temporal evolution of the original magnetic field (blue, top panel), smooth magnetic field (red, top panel) and the magnetic field perturbation for ring 1 obtain subtracting to the original magnetic field signal the smooth signal for the discharge # 11688.

5. Data processing methods

The data are acquired at fast sampling rate in order to follow the rotating modes. The Mirnov signals are oscillating time series from which the overall structure is extracted.

A look at the time traces of Mirnov coil signals may sometimes be sufficient to determine the mode number, particularly when only a single mode is present.

5.1. Fluctuation of raw data analysis (theta-time diagram)

We are trying to identify the mode number (m) and the frequency (f) from data because the analysis of temporal and spatial domain of Mirnov signal sensors can help us of the identification of these quantities.

We have chosen shot # 11688 to explain the analysis of MHD modes using the set of Mirnov coils. Out of 16 probes, 13 probes were operational and were used for the analysis because other 3 probes connections were ionperative.

Loop voltage, plasma current (in the unit of kA) and toroidal magnetic field measured by differents diagnostics can be seen in figure 12 .

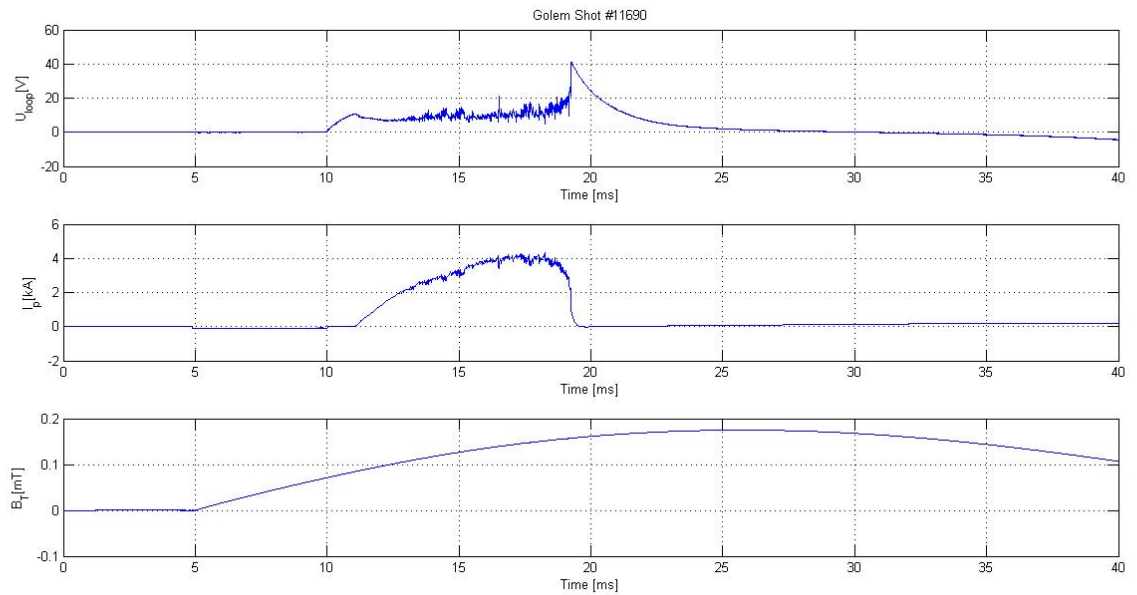


Figura 12: Temporal evolution of whole discharge # 11688, with parameters: loop voltage (U_{loop}), plasma current (I_p) and toroidal magnetic field (B_{tor}).

For this shot and the ring 1 (magnetic sensor at $\theta = 0^\circ$) obtained:

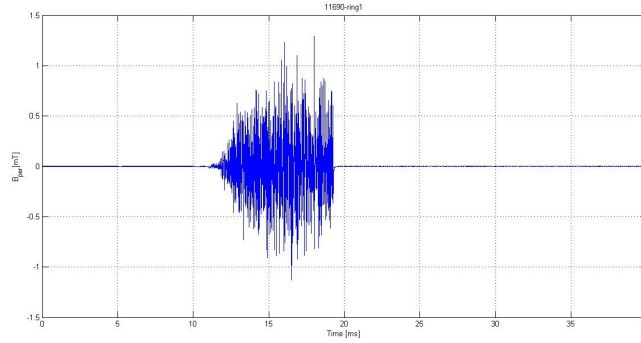


Figura 13: Poloidal magnetic field perturbation obtain by numerical integration of the Mirnov Signal of the ring 1 for the shot # 11688. There are similar signals for all poloidal sensors at the poloidal ring.

For time-space domain, the most common format is a graph with two geometric dimensions: the horizontal axis represents time, the vertical axis the poloidal position of the Mirnov coils; a third dimension indicating the amplitude of perturbed magnetic field at a particular time is represented by the intensity or colour of each point in the image.

Applying this to the oscillation of poloidal magnetic field, one could estimate the mode number of the wave and so determine the mode number of the magnetic island appearing in the plasma projected to poloidal plane. Figure illustrates a typical ohmic discharge contour, with a edge safety factor $q(a) = 3,4$ according to the I_p and B_θ at edge.

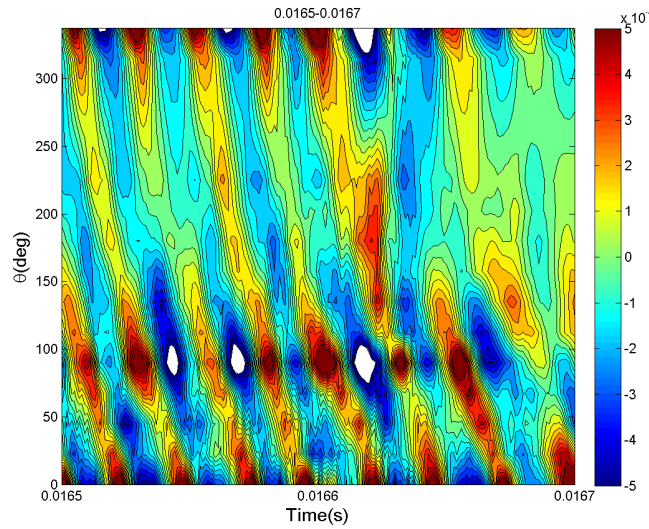


Figura 14: Contour plot of the poloidal magnetic field oscillations in shot # 11688 and with a window time from 0.0165-0.0167 s, where the horizontal and vertical axes correspond to time and poloidal localization of the Mirnov coils. The red and blue region represent the oscillations positive and negative respectively. The color bar on the right side represents intensity of the poloidal magnetic field perturbation in T.

The method for the identification of f and m is count the number of oscillation maxima for one period time given time.

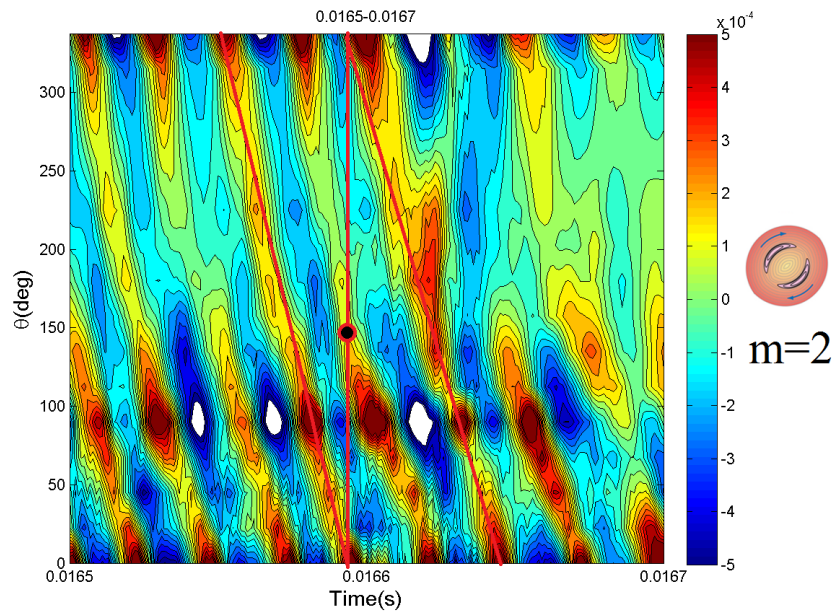


Figura 15: Contour plot of the poloidal magnetic field oscillations in shot #11688 and with a window time from 0.0165-0.0167 s. To determinate m mode, search for a periodicity of a field line (red) and draw a vertical line and count how many maxima are “inside”. The number mode m is equal to the number of maxima (minima) inside+1, in this case $m=2$. The big black dot mark one cut of the vertical line with a maximum inside. At the right we can see a drawing of the $m=2$ rotating island.

5.2. Spectrogram

Fourier analysis [19] is useful to study the spatial and time behavior of a system in wave number and frequency domain. There are several common conventions for defining the Fourier transform \hat{f} of an integrable function $f : \mathbb{R} \rightarrow \mathbb{C}$, for example:

$$\hat{f}(\xi) = \int_{-\infty}^{\infty} f(x) e^{-2\pi i x \xi} dx \quad \text{for every real number } \xi . \quad (20)$$

When the independent variable x represents time (with SI unit of seconds), the transform variable ξ represents frequency (in hertz).

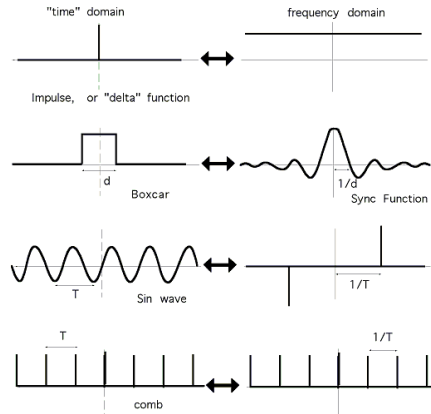


Figura 16: The Fourier transform relates the function's time domain, shown at right, to the function's frequency domain, shown at left. A spike in time is a constant in frequency, a switch on and off in time is a squiggly Bessel function in frequency, a sinusoidal wave in time is a spike in frequency, and a comb of spikes in time is a comb of spikes in frequency. This is true because waves of different frequency add.

Applying this to the oscillation of poloidal magnetic field in a poloidal cross section, one could estimate the mode number of the wave and so determine the MHD mode number appearing in the plasma.

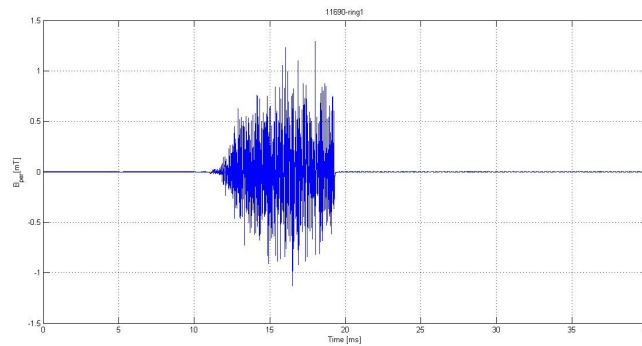


Figura 17: Poloidal magnetic field perturbation obtain by numerical integration of the Mirnov Signal of the ring 1 for the shot # 11688. There are similar signals for all poloidal sensors at the poloidal ring.

However, as only 13 magnetic Mirnov coils were operational, not enough data points are available to do proper Fourier analysis.

The oscillation in time of the poloidal magnetic field at a certain poloidal angle can be studied. This way it is possible to see whether an island is present or not³. As it comes with sinusoidal variation in time of the poloidal magnetic field, one should look for peaks in the frequency spectrum, and this for different time windows. If peaks appear at a certain time span, further investigation of the data at that time is done

For frequency domain, the most common format is a graph with two geometric dimensions: the horizontal axis represents time, the vertical axis is frequency; a third dimension indicating the amplitude of a particular frequency at a particular time is represented by the intensity or colour of each point in the image. This special graph is called spectrogram and is a visual representation of the spectrum of frequencies of the magnetic perturbation.

Here is an example of such a spectrogram. The dark red areas are peaks. The corresponding time intervals have to be further investigated to see if magnetic islands appear.

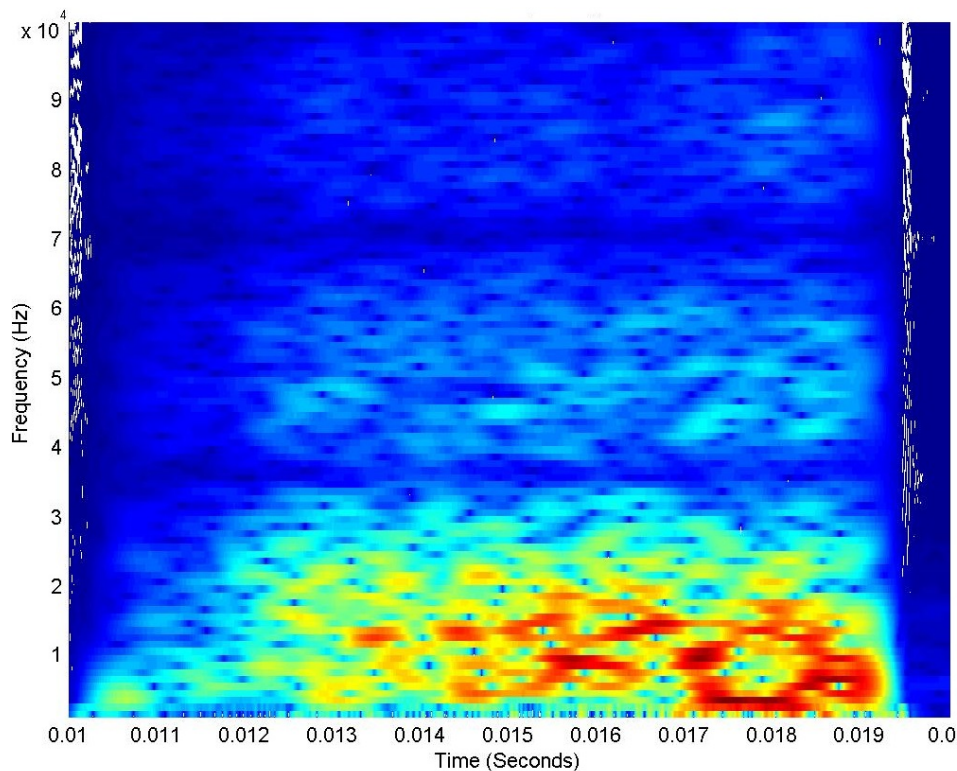


Figure 18: B_θ spectrogram of shot n^0 11767

³This is not necessarily an island not MHD wave, there are a lot of phenomena can appear in the plasma. $|FFT|^2$ gives the spectral distribution of the power of the fluctuation.

5.3. Cross correlation analysis

These analysis is useful in data processing as FFT.

Cross correlation [18] [20] is a standard method of estimating the degree to which two series are correlated. Consider two series $x(i)$ and $y(i)$ where $i=1,2,3,\dots,N$. The cross correlation P at delay Lag is defined as

$$P_{xy}(Lag) = \frac{\sum_{k=1}^{N-|Lag|} (x_{k+|Lag|} - \bar{x}) \cdot (y_k - \bar{y})}{\sqrt{\left[\sum_{k=1}^N (x_k - \bar{x})^2 \right] \cdot \left[\sum_{k=1}^N (y_k - \bar{y})^2 \right]}} \quad \text{for } Lag < 0 \quad (21)$$

$$P_{xy}(Lag) = \frac{\sum_{k=1}^{N-Lag} (x_k - \bar{x}) \cdot (y_{k+Lag} - \bar{y})}{\sqrt{\left[\sum_{k=1}^N (x_k - \bar{x})^2 \right] \cdot \left[\sum_{k=1}^N (y_k - \bar{y})^2 \right]}} \quad \text{for } Lag > 0 \quad (22)$$

If the above is computed for all delays $Lag=1,2,3,\dots,N$ then it results in a cross correlation series of twice the length as the original series.

- x and y represent signals with N data points. Lag has dimension of data point index $t_L = \frac{Lag}{f_{sample}}$. Barred x and y represent averages. Therefore, denominator is geometrical average of signal variances – this causes that P is from $(-1,1)$

There is the issue of what to do when the index into the series is less than 0 or greater than or equal to the number of points. ($i - Lag < 0$ or $i - Lag \geq N$) The most common approaches are to either ignore these points or assuming the series x and y are zero for $i < 0$ and $i \geq N$. The Cross-correlation data processing is excellent for island tracking – normalizes the signals, inhibits fluctuations and brings forward its periodical character.

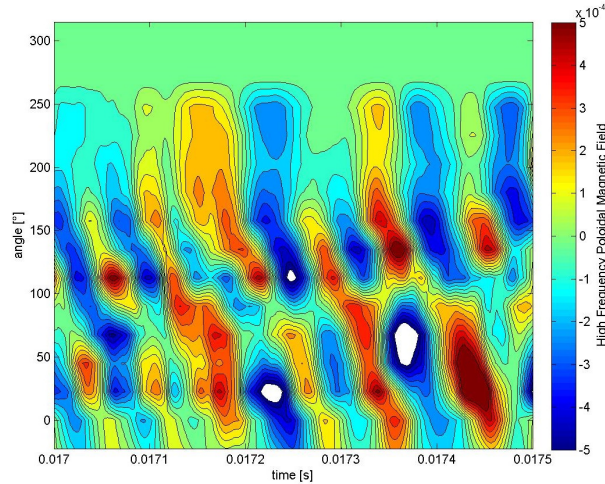


Figure 19: Cross-correlation analysis. A detail of perturbation of shot n^0 11767

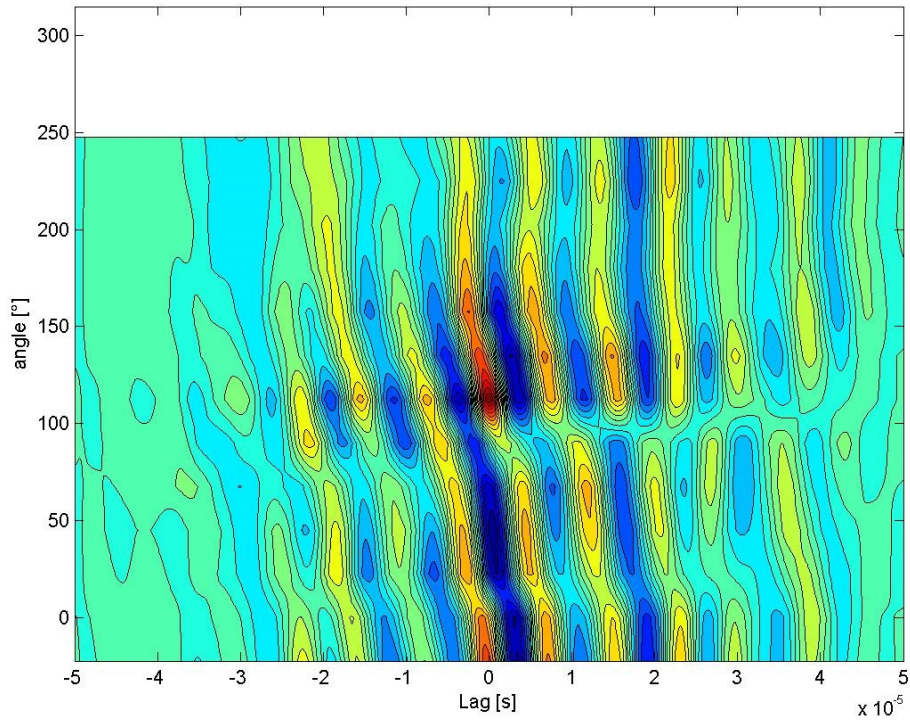


Figura 20: Cross-correlation profile of MHD activity in shot n^0 1176. Begin at 0.017 s and end at 0.0175 s.

6. Results

The mode number of a magnetic island has been directly obtained using θ -time diagram for all discharges and the result are shown⁴ in table 3 .

Cuadro 3: *Determination of m mode in the shots from the Kick-off week session*

Shot #	Island Index	$Time_d[ms]$	$Time_u[ms]$	Mode number m
11686	1	14.7	14.9	2
11687	1	15.1	15.3	2
11688	1	16.4	16.6	2
11689	1	14.8	15.0	2
11690	1	16.1	16.3	2
11691	1	24.1	24.3	2
11691	2	25.8	26	2 or $\ell 3?$
11692	1	25.3	25.5	2
11701	1	14	14.2	2
11702	1	15	15.2	2
11703	1	16.7	16.9	2
11759	1	17.6	17.8	2
11762	1	17.6	17.8	2
11762	2	18.0	18.2	2
11762	3	19.4	19.6	2
11765	1	13.8	14.0	2
11767	1	14.7	14.9	2

It's proven that magnetic island informations are visible from the contour plot of poloidal magnetic field oscillations profile. It's proven that the θ -time diagram is a useful tool for the measurement of magnetic islands .

⁴Same color in discharges indicated the same parameters in the control room

7. Discussion

Energy has played a major role in the development of human civilization. Energy is a vital component to sustain the industrial countries as well as to improve the economic condition of less developed nations. To maintain the balance between the increase of energy supply and the decrease of pollution level, fusion energy has been proposed as a promising candidate for the existing energy options. It has many attractive features in terms of safety, abundance of fuel, and minimal impact on nature.

GOLEM Tokamak is designed to generate plasma using several heating and to confine it by a combination of external and self - induced magnetic fields. A tokamak is a donut-shaped device that uses magnetic fields to confine the plasma. A central solenoid is used to drive the toroidal plasma current. The plasma torus is regarded as a single secondary winding of a transformer.

Tokamak GOLEM is equipped with a set of diagnostic instruments for measuring specific plasma parameters during the discharge. It is desirable to measure these parameters with high precision.

The information on these fluctuations has been retrieved mainly from the measurement of oscillating magnetic fields detected with coils situated inside the plasma for Tokamak GOLEM. MHD instabilities have been successfully observed in Tokamak GOLEM. The detection and interpretation of the MHD fluctuations occurring in tokamak plasma is a challenging task for plasma diagnostics.

The magnetic oscillations, are fluctuations in the magnetic field of the discharge current (particularly the current near plasma boundary) which can be detected outside the plasma ring. A concept which has proved to be of great significance for the stability of plasma in the toroidal magnetic field is that of resonance oscillations. These are oscillations where the helix of the perturbation exactly matches the helix of the confining magnetic field.

The perturbed helix is described by the poloidal and toroidal mode numbers m and n . MHD instabilities in tokamaks may simultaneously occur at different rational surfaces and rotate at either the same or different angular frequencies. Plasma diagnostics (Mirnov coils ring) collect the spatial and temporal information of MHD perturbations, In Tokamak GOLEM MHD studies is by 16 Mirnov coils mounted in a poloidal ring at the same time low values for safety factor are ideal to observe magnetic island as show in the present report, Mode number 2 was observed a lot of times.

Therefore, the first step for an accurate interpretation of the output signals of plasma diagnostics is to choose proper data processing techniques. Fourier transform is considered the universal method for time to frequency domain conversion. The spectrograms show the magnitude of the signal in frequency state for each coil of poloidal arrangement.

8. Appendix

8.1. Appendix I

8.1.1. Safety Factor

Magnetic field in tokamak has a helical shape. The geometry of the magnetic field lines can be described by the safety factor

$$q = \frac{\Delta\Phi}{2\pi} \quad (23)$$

A magnetic field line does not come into the same poloidal position after one toroidal turn, but after several of them, after it covers a toroidal angle $\Delta\Phi$.

The safety factor depends on the geometry of the machine and it varies along the minor radius. For large aspect ratio tokamaks ($\epsilon = \frac{R}{a}$) with circular poloidal cross-section (as in the case of GOLEM), q can be written as:

$$q(r) = \frac{d\chi}{d\psi} = \frac{2\pi r dr B_\Phi}{2\pi R dr B_\theta(r)} = \frac{r}{R} \frac{B_\Phi}{B_\theta(r)} \quad (24)$$

where r and R are the minor and major radii, while B_Φ and B_θ are the toroidal and poloidal magnetic fields.

If we suppose a density current profile like:

$$j(r) = j_0 \left[1 - \frac{r^2}{a^2} \right]^p \quad (25)$$

The poloidal magnetic field generated by the plasma currents B_θ can be expressed as (using

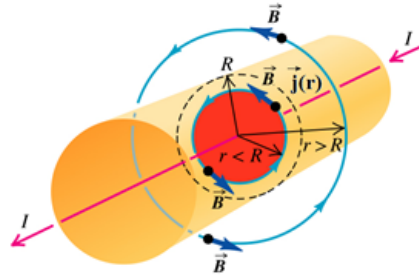


Figura 21

Biot-Savart law, see fig 19):

$$\nabla \wedge \mathbf{B} = \mu_0 \mathbf{j} \rightarrow \oint \underbrace{B_\theta(r)}_{2\pi r B_\theta(r)} \cdot dl = \mu_0 I = \mu_0 \int \int_\Sigma j(r) dS = \mu_0 \int_0^{2\pi} \int_0^r j(r') r' dr' d\theta = \quad (26)$$

$$= \frac{\mu_0 j_0}{2\pi r} \int_0^{2\pi} \int_0^r \left[1 - \frac{r'^2}{a^2} \right]^p r' dr' d\theta = \frac{\mu_0 j_0}{r} \int_0^r \left[1 - \frac{r'^2}{a^2} \right]^p r' dr' = -\frac{a\mu_0 j_0}{r(p+1)} \left(\left[1 - \frac{r'^2}{a^2} \right]^{p+1} - 1 \right) \quad (27)$$

and we can express the poloidal magnetic field by:

$$B_{\theta}(r) = \frac{\mu_0 I_p(r)}{2\pi r} = \frac{\mu_0 I_p(a)}{2\pi r} \left[1 - \left(1 - \frac{r^2}{a^2} \right)^{p+1} \right] \quad (28)$$

where $I_p(r = a) = \frac{2\pi j_0}{p+1}$ is the plasma current which is driven within the radius $r=a$.

The safety factor $q(r)$ can be written as

$$q(r) = q(a) \frac{\frac{r^2}{a^2}}{\left[1 - \left(1 - \frac{r^2}{a^2} \right)^{p+1} \right]} \quad (29)$$

where $q(a)$ is the edge safety factor at edge:

$$q(a) = \frac{2\pi a^2 B_{\Phi}}{\mu_0 R I_p(a)} \quad (30)$$

For the edge of GOLEM tokamak ($a = 85$ mm), we can write

$$q(a) \approx 90,3 \frac{B_{\Phi}(T)}{I_p(a)(kA)} \quad (31)$$

This is true in an ideal case when the plasma column is centralized with the poloidal circumference $a = 85$ mm.

8.2. Appendix II

8.2.1. Frederyk's Scripts

■ dataProc.m

```
1 function out = dataProc(v,AEff,pol)
2 step = 1e-6; %time step in sec
3 %Eliminate offset.
4 av = mean(v(1:5000)); %Look for average value over 5ms
5 vNoOffSet = v-av; %Data - offset
6 %Integrate
7 b = zeros(length(v),1);
8 b(1) = vNoOffSet(1)*step/AEff/pol;
9 for i = 2:length(v)
10     b(i) = b(i-1)+step*vNoOffSet(i)/AEff/pol;
11 end
12 %Subtract moving average to have high freq only
13 out = smooth(b-smooth(b,250),30); %band pass filter
14 end
```

■ getMirnovData.m

```
1 function finalTransp = getMirnovData(numberShot)
2 AEff = [68.93e-4, 140.68e-4, 138.83e-4, 140.43e-4, 68.59e-4, 134.47
3         e-4,134.28e-4, 142.46e-4, 67.62e-4, 142.80e-4, 140.43e-4, 138.02
4         e-4, 76.32e-4, 142.18e-4, 139.82e-4, 139.33e-4]; %in m^2
5 pol = [-1,-1,1,1,-1,1,-1,1,-1,1,-1,-1,-1,-1]; %polarity
6 final = zeros(40000,16);
7 for ring = 1:11
8     [t,v] = golem_data(numberShot,['ring_' num2str(ring)]);
9     final(:,ring+2) = dataProc(v,AEff(ring),pol(ring));
10 end
11 for ring = 15:16
12     [t,v] = golem_data(numberShot,['ring_' num2str(ring)]);
13     final(:,ring-14) = dataProc(v,AEff(ring),pol(ring));
14 end
15 finalTransp = final';
16 end
```

■ **makeCrossCorAlt.m**

```

1 function [] = makeCrossCorAlt(shotNumber, timeWindow)
2 initial = getMirnovData(shotNumber);
3 [rn, cn] = size(initial);
4 twi = round(timeWindow*1e6);
5 tws = length(twi);
6 final = zeros(rn, 2*tws-1);
7 %Choose reference at coil 5
8 ref = initial(7, twi);
9 for i = 1:rn
10     final(i, :) = xcorr(initial(i, twi), ref, 'coeff');
11 end
12 [X, Y] = meshgrid(22.5*(-1:14)', ((-tws+1):(tws-1))/10e6);
13 levels = linspace(-1.0, 1.0, 25);
14 figure; contourf(Y', X', final, levels);
15 xlabel('Lag [s]');
16 ylabel('angle [deg]');
17 title(['Shot ' num2str(shotNumber) ' begin ' num2str(timeWindow(1))
18       's end ' num2str(timeWindow(length(timeWindow))) 's: Cross -
19       correlation diagram'], 'Fontweight', 'bold');
20 saveas(gcf, ['Shot' num2str(shotNumber) '_Begin' num2str(timeWindow
21       (1)) 's_End' num2str(timeWindow(length(timeWindow))) '_CrossCor.
22       jpg']);
23 end

```

■ **makeSpectrogramAlt.m**

```

1 function [] = makeSpectrogramAlt(numberShot, numberCoil, begin, final)
2 close all;
3 %Parameters
4 windowSize = 1000; %Size of windows (number represents indices of
5   input vector)
6 step = 1; %Next window at 'step' away from last one.
7 maxFreqOfInterest = 100000; %Maximum frequency of interest in Hz
8 %Getting data
9 tRange = begin:1e-6:final;
10 X = getMirnovDataCoil(numberShot, numberCoil);
11 XCut = X(round(1e6*begin):(round(1e6*final)+windowSize));
12 hanning = hann(windowSize);
13 spec = zeros(windowSize, length(tRange)+windowSize);
14 %Fast Fourier Transform
15 for t = 1:step:(length(tRange))
16     window = XCut(t:t+windowSize-1); %window of interest
17     window = window-mean(window); %Eliminating off set
18     for w = 1:windowSize
19         window(w) = window(w)*hanning(w); %Multiplying with
20         Hanning function to make sure boudaries are zero
21     end
22 end

```

```

20     fftWindow = fft(window);
21     for amb = t:(t+step-1)
22         spec(:,amb) = fftWindow;
23     end
24 end
25 % Post processing
26 spec = abs(spec);
27 fRange = (1:(windowSize/2+1))/windowSize*1e6;
28 fRangeOfInterest = fRange(1:find(fRange>maxFreqOfInterest,1)); %
    Getting the interesting part
29 specOfInterest = spec(1:find(fRange>maxFreqOfInterest,1),1:(length(
    tRange)));
30 [T,F] = meshgrid(tRange,fRangeOfInterest);
31 surf(T,F,specOfInterest.^(1/3),'edgecolor','none');
32 axis tight;
33 view(0,90);
34 xlabel('Time (Seconds)'); ylabel('Frequency (Hz)');
35 title(['Shot' num2str(numberShot) 'Coil' num2str(numberCoil) '
    Spectrogram'],'Fontweight','bold');
36 end

```

■ makeThetaTime.m

```

1 function [] = makeThetaTime(numberShot,timeWindow)
2 data = getMirnovData(numberShot);
3 [X,Y] = meshgrid(22.5*(-1:14)',timeWindow);
4 levels=linspace(-5e-4,5e-4,20);
5 figure; contourf(Y',X',data(:,round(1e6*timeWindow)),levels);
6 xlabel('time [s]');
7 ylabel('angle [deg]');
8 t = colorbar('peer',gca);
9 set(get(t,'ylabel'),'String','High Frequency Poloidal Magnetic
    Field');
10 title(['Shot' num2str(numberShot) ': Theta - lag diagram'],'
    Fontweight','bold');
11 saveas(gcf,['Shot' num2str(numberShot) '_ThetaTime.jpg']);
12 end

```

■ spectrograms.m

```

1 clc;
2 clear all;
3 close all;
4 shotnumbers = [11762 11765 11767 11768 11769 11770]; %Put the
    numbers of shots here
5 coils = [5]; %Put the coils you're interested in here
6 begin = 0.010; %Begin of time window you want to investigate in
    seconds, should be begin of plasma discharge
7 final = 0.027; %End of time window you want to investigate in
    seconds, should be end of plasma discharge

```

```
8
9 for i = 1:length(shotnumbers)
10     for j =1:length(coils)
11         makeSpectrogramAlt(shotnumbers(i),coils(j),begin,final)
12         saveas(gcf,['Shot' num2str(shotnumbers(i)) 'Coil' num2str(
            coils(j)) 'Spectrogram.jpg']);
13     end
14 end
15 display('Done!')
```



Figura 22

8.3. Appendix III

8.3.1. List of

- Figure I: From Plasma confinement in tokamaks. J. Stockel Institute of Plasma Physics, Academy of Association EURATOM / IPP.CR, Czech Republic
- Figure II: From <http://golem.fjfi.cvut.cz/?p=tokamak>
- Figure IV: From Wesson. Tokamaks. Oxford University Press, Clarendon Press, Oxford, 2004.
- Figure VI: From <http://golem.fjfi.cvut.cz/?p=uvod>
- Figure VII: From <http://golem.fjfi.cvut.cz/?p=uvod>
- Figure VIII: From I. H. Hutchinson, Principles of Plasma Diagnostics, Cambridge University Press, Cambridge, 2002
- Figure XVI: From http://brokensymmetry.typepad.com/broken_symmetry/2008/06/cost-accounting.html
- Figure XXII: From http://www.physics.sjsu.edu/becker/physics51/mag_field.htm

9. Bibliography

Referencias

- [1] World energy outlook 2011, IEA, International Energy Agency OECD, Paris, 2011.
- [2] Climate change 2007 : synthesis report, IPCC, Geneva, Switzerland, 2008.
- [3] F. Francis Chen, Introduction fo Plasma Physics, Plenum Press, New York (1974).
- [4] Wesson. Tokamaks. Oxford University Press, Clarendon Press, Oxford, 2004.
- [5] J. D. Lawson, "Some Criteria for a Power Producing Thermonuclear Reactor", Proceedings of the Physical Society B, Volume 70 (1957), p. 6.
- [6] García Muñoz, Manuel (2006): Fast Response Scintillator Based Detector for MHD Induced Energetic Ion Losses in ASDEX Upgrade. Dissertation, LMU München: Faculty of Physics.
- [7] <http://scitation.aip.org/pop/announcements/Fitzpatrickaps2008.pdf>.
- [8] Former tokamak CASTOR becomes remotely controllable GOLEM at the Czech Technical University in Prague, V. Svoboda, G. Pokol, D. I. Réfy, J. Stöckel, G. Vondrášek, 37th EPS Conference on Plasma Physics P2.111.
- [9] Recent results from GOLEM tokamak. Indeed, you can teach an old dog some new tricks. Í. Ďuran, S. El-Ahmar, O. Grover, M. Gryaznevich, J. Jankowski, J. Kocman, K. Kovařík, T. Markovič, M. A. Martínez-Fuentes, M. Odstrčil, T. Odstrčil, M. Oszwaldowski, T. Růžičková, J. Stöckel, V. Svoboda, G. Vondrášek, 39th EPS Conference & 16th Int. Congress on Plasma Physics P2.059.
- [10] The GOLEM Tokamak for Fusion Education, E. Bromová, I. Duran, O. Grover, J. Kocman, T. Markovič, M. Odstrčil, T. Odstrčil, O. Pluhar, J. Stöckel, V. Svoboda, A. Šindlery, G. Vondrášek, J. Zará, 38th EPS Conference on Plasma Physics (2011) P1.021.
- [11] Golem: <http://golem.fjfi.cvut.cz/?p=tokamak>.
- [12] The Science of JET, John Wesson, JET-R(99)13
- [13] IPP Summer University for Plasma Physics, Max-Planck-Institut für Plasmaphysik.
- [14] Instructions for student measurements on the GOLEM tokamak. Dr. Gergo Pokol, Laszlo Horvath, Csaba Buday, Daniel Imre Réfy
- [15] I. H. Hutchinson, Principles of Plasma Diagnostics, Cambridge University Press, Cambridge, 2002.
- [16] Fluktuace magnetického pole na tokamaku Castor, Ivan Duran, Praha, listopad 2003
- [17] Plasma MHD Activity Observations via Magnetic Diagnostics, Magnetic islands, statistical methods, magnetic diagnostics, tokamak operation. Tomáš Markovič, 2013
- [18] Cross Correlation: AutoCorrelation – 2D Pattern Identification, Written by Paul Bourke, August 1996 .
- [19] Wikipedia: http://en.wikipedia.org/wiki/Fourier_analysis.
- [20] Wikipedia: <http://en.wikipedia.org/wiki/Cross-correlation>.